

Self-Supervised Learning and Opportunistic Inference for Continuous Monitoring of Freezing of Gait in Parkinson’s Disease

Shovito Barua Soumma, *Student Member, IEEE*, Kartik Mangipudi, Daniel Peterson, Shyamal Mehta, and Hassan Ghasemzadeh, *Senior Member, IEEE*

Abstract—Parkinson’s disease (PD) is a progressive neurological disorder that impacts the quality of life significantly, making in-home monitoring of motor symptoms such as Freezing of Gait (FoG) critical. However, existing symptom monitoring technologies are power-hungry, rely on extensive amounts of labeled data, and operate in controlled settings. These shortcomings limit real-world deployment of the technology. This work presents *LIFT-PD*¹, a computationally-efficient self-supervised learning framework for real-time FoG detection. Our method combines self-supervised pre-training on unlabeled data with a novel *differential hopping windowing* technique to learn from limited labeled instances. An opportunistic *model activation* module further minimizes the power consumption by selectively activating the deep learning module only during active periods. Extensive experimental results show that *LIFT-PD* achieves a 7.25% increase in precision and 4.4% improvement in accuracy compared to supervised models while using as low as 40% of the labeled training data used for supervised learning. Additionally, the model activation module reduces inference time by up to 67% compared to continuous inference. *LIFT-PD* paves the way for practical, energy-efficient, and unobtrusive in-home monitoring of PD patients with minimal labeling requirements.

Index Terms—Parkinson’s Disease, Self Supervised Learning, Wearable Sensors, Freezing of Gait, Movement Disorder, data scarcity, class imbalance

I. INTRODUCTION

PARKINSON’S disease (PD) is a progressive neurological disorder affecting 7–10 million people worldwide, significantly impacting their quality of life. Freezing of Gait (FoG), a transient inability to produce effective steps during walking [1], is one of the most debilitating symptoms of PD, leading to poor mobility, increased risk of falls and injuries, and reduced quality of life. While treatments like levodopa

can sometimes reduce the severity of freezing episodes, their effectiveness is often incomplete and variable, diminishing over time [2]. Compensatory treatments such as on-demand cueing require patient or companion initiation, which can be challenging in time-sensitive or anxiety-provoking situations that trigger freezing [3]. Identifying FoG events and, more importantly, the time leading up to a FOG event could result in early deployment of on-demand cues to help reduce the severity of a freezing event [4].

In recent years, wearable technology and machine learning (ML) algorithms have emerged as promising tools for continuous monitoring and management of PD symptoms, including gait disturbances and tremors [5]–[7]. However, real-world deployment of these technologies for continuous monitoring and intervention has remained a significant research challenge. One major hurdle is the scarcity of labeled data essential for training robust ML models, particularly in PD, where symptom manifestation is highly individualized. Data annotation requires considerable time and expertise, limiting the availability of accurate and diverse datasets [8].

Detecting FoG using a patient-independent model is a complex task due to significant inter- and intra-variability in patients’ gait patterns. Previous research on FoG detection relied on multiple sensors, extensive feature engineering, patient-specific data collection, and model retraining [9]–[11]. To address these challenges, we present an innovative label-efficient, patient-independent, and robust self-supervised learning framework, *LIFT-PD* (Label-efficient In-home Freezing-of-gait Tracking in Parkinson’s Disease), for detecting FoG events in real-time. Our extensive results demonstrate that the proposed self-supervised model achieves comparable performance to baseline supervised models, despite using much fewer labeled instances and in an unsupervised fashion. Furthermore, we devise a novel opportunistic-based lightweight algorithm that reduces the complexity of model execution and processing time, paving the way for implementation in a stand-alone wearable system for real-time symptom monitoring.

II. RELATED WORK

Prior work can be summarized into two categories including (1) self-supervised learning (SSL) for motion analysis; and (2) automatic detection of FoG events.

Date submitted: October 09, 2024.

Shovito Barua Soumma, Daniel S. Peterson, and Hassan Ghasemzadeh (e-mail: shovito@asu.edu, daniel.peterson1@asu.edu, hassan.ghasemzadeh@asu.edu) are with the College of Health Solutions, Arizona State University, Phoenix, AZ 85004, USA. Daniel S. Peterson and Hassan Ghasemzadeh are both Associate Professors in the College of Health Solutions.

Kartik Mangipudi, Assistant Professor of Neurology at the University of Florida, Jacksonville, FL, USA (e-mail: kartik.mangipudi@jax.ufl.edu) and Shyamal H. Mehta, Associate Professor of Neurology at the Mayo Clinic, Scottsdale, AZ, USA. (e-mail: Mehta.Shyamal@mayo.edu)

¹The source code is available at: <https://github.com/shovito66/LIFT-PD>

TABLE I: Summary of Recent FoG Detection Works. FI:Freezing Index, SP: Stride Peak, STD:Standard Deviation, SD: Subject Dependent, SI: Subject Independent, LOOCV: Leave-One-Out Cross-Validation

Study	Method	Sensor (Number) (Position)	Preprocessing/ Extracted Features	Validation	Contribution
[9]	CNN and Transformer (Supervised)	Accelerometer (1) (Left Waist)	Resample, Filtering, FFT, FI	LOSO CV (SI)	Transformer and CNN based methodologies for FoG detection, along with a clustering approach for FoG episode analysis
[12]	Multihead CNN (Supervised)		×	Hold Out (SI)	Light algorithm for real-time FoG detection using raw sensors data.
[5]	Supervised ML	IMU (2) (Shin)	Time & Frequency Domain Features	10 Fold CV, LOSO train-test 70-30%	Detect and predict FoG considering the im- pact of dopaminergic therapy on performance.
[11]	Semi Supervised 3 Layers	IMU (1) (Ankle)	Filtering, 3 Features (FI, SP, STD)	LOSO (SD)	Adapting FoG classifier’s parameters in real- time with unlabeled data
[10]	Supervised, transfer learning	IMU (2) (Left-Right Ankle)	Filtering, Data Augmentation	LOOCV (SI)	One-class classifier for FoG detection using only normal gait data

The SimCLR SSL technique was originally designed for computer vision tasks, [13], but was later adapted for human activity recognition (HAR) using a transformer-based encoder method [14]. Although MLPs are not popular for vision or language datasets, they are effective in making predictions on tabular health data [15], [16]. Previous work also introduced transfer learning [16], data augmentation technique and re-sampling, which are efficient in scenarios with limited labeled data [17]. The efficacy of self-supervised learning in medical time series analysis has been demonstrated, emphasizing its role in data augmentation and contrastive pair formation [18].

The detection of FoG events in PD has been the subject of extensive research, often involving multimodal datasets. In particular, prior work explored the effectiveness of different sensor modalities such as gait acceleration, electroencephalogram (EEG), electromyography (EMG), and skin conductance (SC) in FoG detections [19]. Furthermore, researchers used an LSTM-based model combining acceleration and synthetic EEG data [20].

Table I summarizes recent PD studies on FoG detection. LIFT-PD overcomes key limitations of these studies, such as limited generalizability, reliance on extensive labeled data, and high computational complexity. In contrast, our proposed method, LIFT-PD, addresses these limitations by introducing a self-supervised learning framework tailored for real-time FoG detection using a single accelerometer sensor.

III. LIFT-PD SYSTEM DESIGN

Training robust deep learning (DL) models typically requires large amounts of labeled data, which can be challenging to obtain, especially for tasks like freezing of gait (FoG) detection in elderly. To address this issue, LIFT-PD employs self-supervised learning to utilize unlabeled data during training. Another challenge that we face while designing ML models for FoG detection is that FoG events are sparse, resulting in an imbalanced dataset with a significantly lower proportion of FoG episodes compared to non-FoG activities. To mitigate this challenge, we incorporate the Differential Hopping Windowing (DHW) Technique during data preprocessing, which applies variable overlaps for FoG and non-

FoG instances, thereby enhancing the model’s ability to learn from the underrepresented class. Finally, an opportunistic-based lightweight algorithm is introduced to reduce execution complexity, allowing for implementation in stand-alone wearable devices (Section III-B).

A. Problem Modeling by Self-Supervised Learning (SSL)

The FoG event detection problem is framed as a multivariate time-series classification task. At each time stamp t , the input raw signal is represented as a vector $\mathbf{x}_t = [x_t^1, x_t^2, x_t^3]$ where $\mathbf{x}_t \in \mathbb{R}^{C=3}$ and \mathbf{C} corresponds to the three-channel (x, y, z) accelerometer data. These raw signals are then combined into a matrix, $\mathbf{X} = [x_1, x_2, \dots, x_T] \in \mathbb{R}^{T \times C}$. After applying the DHWT method, the signals are transformed into N number of training frames (windows) ($\mathbf{X} \in \mathbb{R}^{T \times C} \rightarrow \mathbf{X}_W \in \mathbb{R}^{N \times T' \times C}$) where $x_{w_i} \in X_W$ represents i^{th} window, T' is the windowing time length and $\mathbf{X}_W = [x_{w_1}, x_{w_2}, \dots, x_{w_N}]$.

$$D : \mathbf{X} \in \mathbb{R}^{T \times C} \rightarrow \mathbf{X}_W \in \mathbb{R}^{N \times T' \times C}$$

$$\mathbf{X}_W = [x_{w_1}, x_{w_2}, \dots, x_{w_N}]$$

The ultimate goal is to correctly assign a label $y \in \{0, 1\}$ to each window, where $y = 1$ represents ‘‘FoG’’ and $y = 0$ represents ‘‘non-FoG’’.

LIFT-PD uses SSL for FoG detection in two steps: learning contextual representations from raw signals using a 1D CNN model, followed by performing the downstream FoG detection task. In this paper, raw accelerometer signals are used as physiological signals and the downstream task is binary ‘Freezing of Gait’ detection. In the following subsections, we describe in detail the two main components of our SSL approach:

1) *Pretext Task (Signal Reconstruction)*: During pre-training, a 3-layer neural network model with an encoder is trained using SSL. Random segments of fixed length m are masked from each window, x_{w_i} by replacing them with zeros. The model is then trained to predict these masked values. as shown in Fig. 1 (Part 1). This whole training process does not need any labeled data. The masked signal data $\hat{X}_W \in \mathbb{R}^{N \times T'}$, is defined by $\hat{X}_W = \text{mask}(X_W, m)$ where $\hat{x}_{w_i} \in \hat{X}_W$

The encoder $f_\theta : \mathbb{R}^{N \times T'} \rightarrow \mathbb{R}^{N \times D}$ reconstructs the original signal from the masked windows, producing a lower

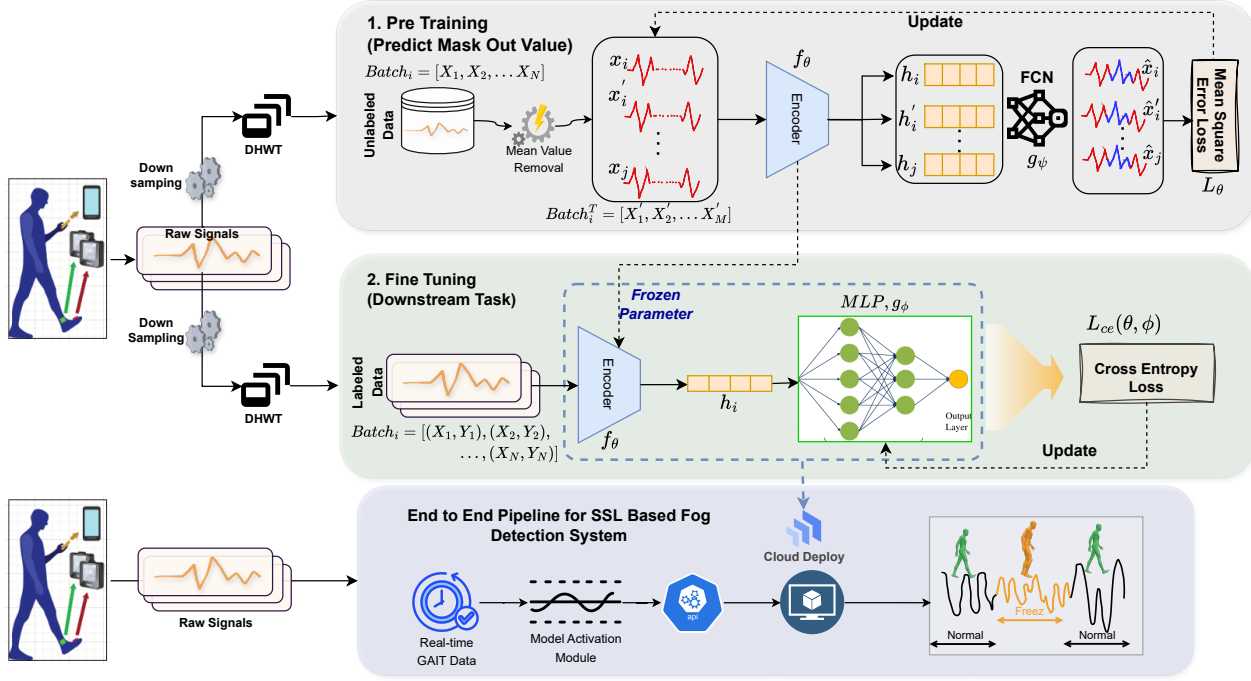


Fig. 1: Self-Supervised training pipeline for real-time FoG detection. **Pretrain:** Encoder reconstructs masked signal segments, outputting predicted values h_i for missing data. **Fine-tuning:** Encoder weights are frozen while the MLP is optimized using cross-entropy loss on labeled data. **End-to-End Pipeline:** The trained model is integrated into a real-time system, where *model activation module (MAM)* selectively activates the computationally intensive FoG detection model for energy-efficient, long-term monitoring.

dimensional hidden representation $H \in \mathbb{R}^{N \times D}$, where $h_i \in \mathbb{R}^D \leftarrow f_\theta(\hat{x}_{w_i})$. These are passed through a fully connected network $g_\psi(\cdot)$ to predict the masked segments represented as $\hat{x} = g_\psi(h_i)$. The encoder minimizes the reconstruction loss L_θ using mean squared error (MSE) defined as $L_\theta = \frac{1}{N_m} \sum_{j=1}^{N_m} (\hat{x}_j - x_{p(j)})^2$, where N_m is the total number of masked points, \hat{x}_j is the prediction for the j -th masked point, and $x_{p(j)}$ is the original input value, whose position is $p(j)$ in the segmented signal windows.

2) *Downstream Task (FoG Classification):* After pre-training, a Multilayer Perceptron (MLP) $g_\phi : \mathbb{R}^{N \times D} \rightarrow Y$, is introduced on top of the encoder for binary FoG detection. The MLP maps the learned embeddings H to FoG or non-FoG labels Y , represented as $\hat{Y} = g_\phi(H) = g_\phi(f_\theta(X_W))$, where f_θ is the pre-trained encoder with parameters θ .

The fine-tuning step is supervised, using a small amount of labeled data, with the encoder weights frozen and only the MLP layers trained with a lower learning rate as shown in Fig. 1 (Part 2). We minimize the binary cross-entropy loss $L_{ce}(\theta, \phi)$ for the downstream task defined as $L_{ce}(\theta, \phi) = -\frac{1}{N} \sum_{i=1}^N [y_i \log(\sigma(\hat{y}_i)) + (1 - y_i) \log(1 - \sigma(\hat{y}_i))]$, where N is the total number of windows, y is an indicator variable (1 for FoG, 0 for non-FoG), σ is the sigmoid function, and $\hat{y} \in \hat{Y}$ is the output of the classifier $g_\phi(h_i)$.

B. Opportunistic Inference

To optimize power consumption and computational resources for real-life in-home PD monitoring using wearable devices, we propose an opportunistic-based naive algorithm as a *model activation module (MAM)*. This module differentiates

between active and inactive periods, activating the computationally heavy self-supervised learning (SSL) FoG detection model only during identified active intervals, as shown in Fig. 2. The activation module filters out inactive windows,

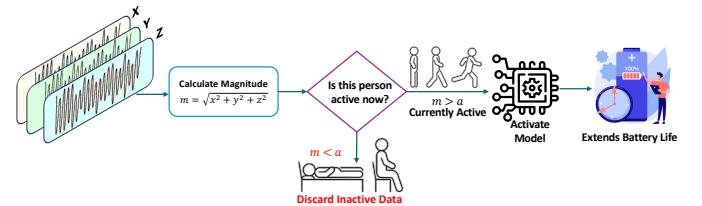


Fig. 2: **Model Activation Module:** Activity threshold-based triggering mechanism for computational offloading and battery life extension in wearable FoG detection system.

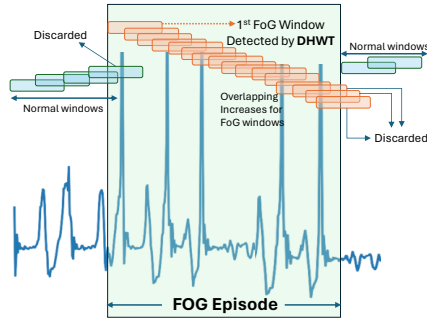
ensuring the SSL model is selectively executed only when activity is detected, significantly reducing power consumption and avoiding false positives during inactivity. During inactive periods, simpler methods handle the data by comparing the magnitude of the current incoming signal, leading to more efficient power utilization. For each window $i \in [1, N]$, the magnitude M_i of the 3D accelerometer is calculated as $M_i = \frac{1}{T'} \sum_{t=1}^{T'} \left\| \sqrt{a_{x,t}^2 + a_{y,t}^2 + a_{z,t}^2} \right\|$ where a_x, a_y , and a_z are the acceleration signal along each axis. A window is considered active if $M_i \geq \alpha$, where α is a predefined threshold (Eq. 1), otherwise MAM discards it.

$$\begin{cases} 1 \text{ (active)} & \text{if } M_i \geq \alpha \\ 0 \text{ (inactive)} & \text{otherwise} \end{cases} \quad (1)$$

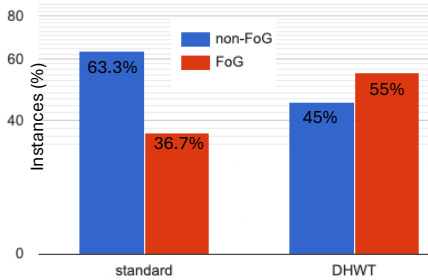
The threshold was chosen to discard windows without degrading SSL algorithm performance. Finally, the effect of the magnitude threshold was evaluated separately during the inference time (Sec. IV-D).

C. Imbalanced Training Data Mitigation

Our proposed dataset generation method (DHWT) effectively handles imbalanced datasets without the need for additional preprocessing, balancing informative features with computational efficiency for real-time deployment on wearable devices. We segment raw sensor data into short, overlapping windows, adjusting the overlap based on activity type. For



(a) DHWT: Overlapping size increases.



(b) Balanced class distribution using DHWT

Fig. 3: DHWT segmentation process for training set (a); FoG proportion using standard vs. DHWT segmentation (b).

instance, in our experimental evaluation shown in Fig. 3a, we applied a 50% overlap for non-FoG periods and a 75% overlap for FoG episodes during training. During inference, windows are segmented using standard, non-variable overlaps to simulate real-world conditions where FoG episodes are not pre-identified. Using fixed-length overlaps typically results in an unbalanced training set, as illustrated in the left bar of Fig. 3b, with 63.3% non-FoG and 36.7% FoG instances. In contrast, the DHWT segmentation approach achieves a more balanced distribution, as shown in the right bar of the same figure, with non-FoG and FoG data at 45% and 55%, respectively. For test set generation, standard segmentation with a fixed 50% overlap (advancing every 1.5 seconds) mimics actual operating conditions, processing data from the preceding 3 seconds.

D. Dataset

The dataset for this study is the publicly available tDCS FoG dataset, comprising movement data from PD subjects in

both medicated ('On') and unmedicated ('Off') states during Freezing of Gait (FoG) provocation protocols [21]. Data were collected using a 3D accelerometer attached to the lower back, recording at 128 Hz, resulting in 1132 FoG episodes (285 minutes total) and 15.3 hours of recording. Each FoG episode was videotaped and annotated by experts. The demographic and clinical characteristics of the subjects are summarized in Table II. The dataset contains events labeled as "Normal" or "Freezing of Gait" (FoG). The distribution of these events is summarized in Table III. The sessions followed the FoG provocation protocol as described in seminal studies by Reches et al. [22] and Manor et al. [23], and originally defined by Ziegler et al. [24].

TABLE II: Summary of patient characteristics

Characteristics	Overall	Medication	
		On	Off
Male (Female)	8 (32)	7 (31)	6 (20)
Age, mean (SD)	69.5 (7.75)	70.9 (6.5)	68 (8.3)
UPDRS ON, mean (SD)	34.27 (12.7)	34.27 (12.7)	–
UPDRS OFF, mean (STD)	42.88 (12.99)	–	42.88 (12.99)
NFOGQ, mean (STD)	17.12 (7.57)	–	–
Years Since DX mean(SD), [min, max]	10.5 (5.9), [1, 23]		

TABLE III: Event distribution during FoG provocation trials

Event Type	Medication (%)		Total (%)
	On	Off	
Normal	28.01	35.41	63.42
FoG	18.73	17.86	36.59

We resampled the data to 40 Hz, which is considered an effective frequency for recognizing human activity through accelerometers in both healthy individuals and PD patients, including those experiencing Freezing of Gait (FoG) episodes. This frequency captures the typical freeze band (3-8 Hz) while reducing memory load and computational complexity.

E. Mean Value Removal and Labeling

After segmentation, we perform minimal pre-processing on each window by removing the mean value from each of the sensor axes (e.g., x, y, z). This centering of the data mitigates sensor bias and reduces computational complexity. Finally, we assign labels to the windows based on their content: non-FoG for windows containing only non-FoG data, and FoG for windows with at least 50% FoG data. Any windows containing a mix of both activities are discarded to ensure clear classification during the machine learning stage. This minimal preprocessing approach prioritizes real-time performance while preserving features relevant for FoG detection.

F. Leave One Group Out (LOGO)

In order to evaluate the subject-independence, we perform a leave-one-group-out cross-validation. The whole tDCS dataset is divided into two groups, each of them consisting of randomly chosen 20 patients. The two groups are generated so that patients in each group have similar characteristics in terms of

Algorithm 1: Activity Threshold Optimization Algorithm for Prolonged Battery Life

Input: X : Set of inference data frames,
 $[\alpha_{start}, \alpha_{final}]$: Initial and final threshold,
 P_0 : Baseline performance metric,
 $f(\cdot)$: Inference Model,
 $A(\cdot)$: returns magnitude for $x_i \in X$
Output: α_{opt} : Optimal activity threshold,
 X_{opt} : Active frames for (α_{opt})
Initialization $\alpha \leftarrow \alpha_{start}$
while $\alpha \leq \alpha_{final}$ **do**
 $X_{active} = \{x_i \in X \mid A(x_i) \geq \alpha\}$ \triangleright Set of active frames;
 $N_\alpha \leftarrow |X_{active}|$ \triangleright Size of active frames;
 $P \leftarrow f(X_\alpha)$
 if $|P - P_0| \leq \theta$ **then**
 $\alpha \leftarrow \alpha + \delta\alpha$
 else
 $\alpha_{opt} \leftarrow \alpha$;
 $X_{opt} = \{x_i \in X \mid A(x_i) \geq \alpha_{opt}\}$;
 break;
 end
end
return α_{opt}, X_{opt}

age, duration of symptoms, and UPDRS. Hence, the patient-independent model is trained using 20 patients from each group using SSL, while the left-out group is stripped of its labels for validation. The classification performance for the left-out groups of patients is then evaluated and compared with our baseline supervised model. This procedure is repeated for each group within the dataset, conducted three times, and the results are averaged to ensure reliability and robustness in our findings.

G. Model Development & Experimental Setup

For our downstream task, we devise a 5-layer 1D Convolutional Neural Network (CNN) architecture in LIFT-PD (Fig. 4), allowing us to use raw sensor data without extensive feature engineering. The model consists of an encoder block for feature extraction and a classification block for FoG detection. The encoder block has five 1D convolutional layers

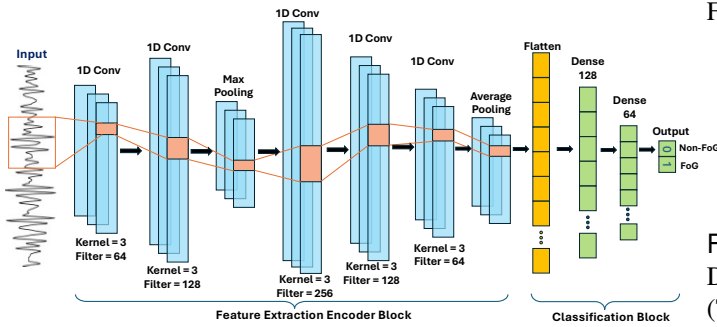


Fig. 4: Architecture of stacked 1D CNN model. Input to the model is 3-minute raw sensor data.

(filters: 64, 128, 256, 128, 64; kernel size: 3; ReLU activation) with max-pooling (pool size: 2) after the second layer and global average pooling (pool size: 2) after the fifth layer to

downsample feature maps, reducing complexity. The flattened output is passed through an MLP with two dense layers (units: 128, 64; ReLU activation; dropout: 0.4 after the first layer) for binary classification, with a final dense layer (unit: 1; sigmoid activation) providing the FoG detection output.

The model was trained in two phases: pre-training and fine-tuning. In the pre-training phase, the encoder was trained for 70 epochs with a batch size of 64, using the Adam optimizer set to a learning rate of 0.01 and a decay of 0.001. During the fine-tuning phase, the additional dense layers were randomly initialized. The model was fine-tuned on labeled data for 40 epochs, maintaining the same batch size but with a reduced learning rate of 0.0001 for the classification task. The use of a lower learning rate (0.0001) during the fine-tuning phase is a common practice when working with pre-trained models. This lower learning rate helps preserve the learned features from the pre-training phase and ensures gradual adjustments, avoiding the drastic loss of previously learned representations.

All experiments (pre and post-processing) were performed on a computer with an Apple M2 Pro chip, which includes a 16-core Neural Engine, and 16 GB of unified memory. Training, optimization, and testing of the classification model were performed in Python (3.8), using the Keras (2.4), and TensorFlow (2.3) libraries.

H. Performance Measures

To evaluate the performance in FOG detection at window-level of our proposed framework and those reproduced from the state-of-the-art approaches, commonly used metrics were calculated and reported.

In this binary classification problem (FoG or non-FoG), performance metrics include sensitivity, specificity, F1 score, and AUC of receiver operating characteristics. We extensively evaluated our proposed system using these metrics, comparable to other state-of-the-art methods. True positives (TP) are correctly identified FoG windows, while false positives (FP) are non-FoG windows incorrectly labeled as FoG. False negatives (FN) are real FOG windows not recognized, and true negatives (TN) are correctly classified non-FoG instances. Fig. 5 schematically describes these metrics.

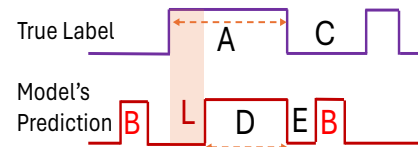


Fig. 5: A: FoG Episode, B: False Positive, C: Normal Episode, D: Detected FoG Episode (TP), E: Detected Normal Episode (TN), L: Latency

Sensitivity/Recall measures the ratio of correctly detected FOG windows and specificity measures the ratio of correctly identified non-FoG windows. Precision evaluates the model's ability to avoid false positives. The F1 score is the harmonic mean of sensitivity and precision which is used to assess performance on the imbalanced dataset [25].

I. FoG Detection Post-processing

For further evaluation of our LIFT-PD framework, a post-processing analysis was performed using predictions and class labels. The performance of *true FoG episode (TFE)* detection was performed by analyzing groups of consecutive windows with the presence of freezing episodes, besides the window-level FoG detection.

1) *FoG Episode*: In our study, we assessed the detection of FoG episodes—defined as consecutive windows labeled as FoG—by computing both the percentage of episodes detected and the proportion of FoG accurately identified within each episode. An episode is considered detected if at least one window within it is correctly identified. FoG episodes were categorized into three groups: short (< 6 seconds), medium (6 – 12 seconds), and long (> 12 seconds).

Then we calculated the percentage of FoG episodes detected across the entire dataset and for each duration group. We also measured the proportion of accurately detected FoG windows within each episode (Fig. 5D), defined as $D_{FoG}(\%) = \frac{n_{detected}}{n_{total}}$, where $n_{detected}$ represents the number of detected FoG windows, and n_{total} is the total FoG windows in that episode.

For false FoG episodes, we calculated the minimum distance between each falsely detected episode (Fig. 5B) and the nearest true FoG window (Fig. 5A) to understand the proximity of false positives to actual FoG occurrences. Finally, we evaluated FoG detection latency, defined as the time difference between the onset of an actual FoG episode and the detected FoG episode (Fig. 5L). This metric reflects the algorithm’s responsiveness in identifying FoG events, which is crucial for the timely intervention and management of PD patients.

2) *Computational Complexity*: To evaluate the feasibility of deploying our LIFT-PD framework on low-resource wearable devices, we performed several analyses. We assessed training and testing times for different input sizes to identify the optimal training size for the self-supervised pre-text task using varying amounts of unlabeled data. Post-training, we measured inference times across different input sizes to gauge real-time performance.

We also analyzed memory requirements for storing input sensor data and model parameters, ensuring suitability for resource-constrained devices. To optimize power consumption and enable long-term in-home monitoring, we introduced an Activity Threshold Optimization (ATO) algorithm (Algorithm 1), activating the FoG detection model only during active periods. Assuming that the performance function P and the computation of active windows N_α can be performed in constant time, the overall runtime excluding the inference model is $O(N \cdot \frac{\alpha_{max}}{\delta\alpha})$. Including the inference model’s runtime $O(M)$, where M is the process time of a single active window, the adjusted complexity becomes $O((M + N) \cdot \frac{\alpha_{max}}{\delta\alpha})$. In the best-case scenario, where the optimal threshold α_{opt} is found in the first iteration, the runtime is $O(N)$.

IV. RESULTS

A. Performance Analysis

We evaluated the performance of the LIFT-PD framework using mainly sensitivity, and specificity along with some other

matrices (percentage of detected episode, latency, precision, F1 score, and AUC of the ROC curve), comparing it against a baseline supervised model with the same architecture and parameters. This comprehensive evaluation highlights the benefits and potential limitations of our self-supervised learning (SSL) approach for real-time FoG detection.

Table IV summarizes the metrics, showing that the SSL model achieved notable improvements: a 7.25% increase in average precision, 4.4% in accuracy, and 6.5% in specificity compared to the baseline supervised model. Importantly, the SSL model maintained consistent recall/sensitivity (84%) with the baseline, ensuring that the detection of FoG episodes was not compromised despite reduced supervision. The F1 score, which balances precision and recall, was higher by about 3.95% in the SSL model, indicating better overall performance in detecting FoG episodes.

Group 2 outperformed Group 1 in all metrics. Group 1’s lower precision (0.66) was due to more false positives from a higher proportion of FoG events. The DHW technique with SSL mitigated data imbalance, enhancing performance despite class imbalances in Group 1. The ROC curves in Fig. 6 showed

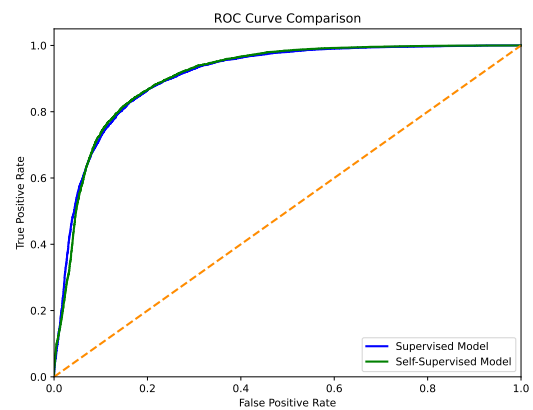


Fig. 6: Receiver Operating Characteristic (ROC) curves for supervised and self-supervised models

that the SSL model had a slightly larger area under the curve (0.908) than the supervised model (0.9078), indicating better FoG classification performance. The close proximity of the AUC values between the two models highlights the robustness of our SSL approach in achieving comparable performance to the supervised baseline, despite leveraging limited labeled data during training.

1) *Generalizability of DHWT*: We expanded our analysis to Daphnet [26] and two activities from MotionSense [27] (as a binary classification), in addition to the primary tdcx dataset. The results show an increase in training time across the datasets due to class imbalance handling, while the inference time remained stable. DHWT significantly improved precision, F1-score, and specificity in datasets with class imbalance, confirming its effectiveness across diverse conditions. Daphnet showed a 161% boost in precision and a 108% improvement in specificity. These results support the generalizability of DHWT without compromising computational efficiency (Table VI).

2) *Robustness Across Diverse Subjects*: To ensure generalizability, we split the dataset (N=40) into diverse groups based

TABLE IV: Performance of proposed *LIFT-PD* framework. Key Metrics Defined: PREC: Precision, REC: Recall, SENS: Sensitivity, ACC: Accuracy, SPEC: Specificity, DFE: Detected FoG Episodes, DFW: Detected FoG Windows, STD: Standard Deviation. Performance metrics for the baseline supervised model are presented within parentheses ().

Group	Prec	Rec/Sens/DFW	F1 Score	Acc.	Spec.	Loss	DFE	DFW
1	0.66 (0.61)	0.82 (0.82)	0.73 (0.70)	0.81 (0.77)	0.81 (0.75)	0.19 (0.23)	86.65% (86.7%)	81.6% (82.0%)
2	0.82 (0.77)	0.86 (0.86)	0.84 (0.81)	0.84 (0.82)	0.83 (0.78)	0.16 (0.19)	89.35% (90.1%)	86.1% (86.1%)
Avg.	0.74 (0.69)	0.84 (0.84)	0.79 (0.76)	0.825 (0.79)	0.82 (0.77)	0.18 (0.21)	88.00% (88.4%)	83.85% (84.1%)
Min	0.66 (0.61)	0.82 (0.82)	0.73 (0.70)	0.81 (0.77)	0.81 (0.75)	0.16 (0.19)	86.65% (86.7%)	81.60% (82.0%)
Max	0.82 (0.77)	0.86 (0.86)	0.84 (0.81)	0.84 (0.82)	0.83 (0.78)	0.19 (0.23)	89.35% (90.1%)	86.10% (86.1%)
STD	0.11 (0.11)	0.03 (0.03)	0.08 (0.08)	0.02 (0.03)	0.01 (0.02)	0.02 (0.03)	1.91 (2.4)	3.18 (2.9)

TABLE V: Performance comparison across diverse groups. Performance metrics for the baseline supervised model are presented within parentheses ().

Group	Test Group	Pre	Rec	F1	Spec	Acc
Severity (40)	Severe	0.71 (0.7)	0.81 (0.79)	0.75 (0.74)	0.79 (0.79)	0.8 (0.79)
	Mild (14)	0.78 (0.78)	0.81 (0.81)	0.80 (0.79)	0.85 (0.84)	0.83 (0.83)
Gender (40)	Female	0.78 (0.67)	0.75 (0.77)	0.76 (0.72)	0.84 (0.71)	0.80 (0.77)
	Male (32)	0.71 (0.74)	0.67 (0.64)	0.69 (0.68)	0.83 (0.86)	0.77 (0.77)
Age (40)	Old (20)	0.80 (0.75)	0.71 (0.71)	0.75 (0.74)	0.86 (0.82)	0.80 (0.78)
	Mid-age	0.70 (0.66)	0.80 (0.79)	0.74 (0.72)	0.82 (0.79)	0.81 (0.79)
Medication	On	0.82 (0.78)	0.79 (0.72)	0.81 (0.75)	0.84 (0.82)	0.86 (0.81)
	Off	0.78 (0.70)	0.8 (0.74)	0.79 (0.72)	0.79 (0.72)	0.82 (0.78)
Random (40)	1 (20)	0.66 (0.61)	0.82 (0.82)	0.73 (0.70)	0.81 (0.75)	0.81 (0.77)
	2 (20)	0.82 (0.77)	0.86 (0.86)	0.84 (0.81)	0.83 (0.78)	0.84 (0.82)

TABLE VI: Performance comparison of DHWT across datasets. The second row shows relative improvement over the baseline.

Dataset	Train Time	Test Time	Pre	F1	Spec	Acc
tdcs	1.8s	0.94s	0.74	0.8	0.82	0.83
	↑88%	(0.92s)	↑7.2%	↑5.3%	↑6.5%	↑5.1%
Daphnet	0.14s	0.134s	0.55	0.44	0.94	0.87
	↑42%	(0.132s)	↑161%	↑42%	↑108%	↑71%
MotionSense	0.08	0.022s	1	0.99	1	0.99
	↑142%	(0.024s)	↑3.1%	↑2.5%	↑1.2%	↑1.22%

on key characteristics such as severity (Mild N=14), gender (Male N=32) and age (Mid-age N=20). These groups were deliberately formed to include outliers and reflect real-world diversity, ensuring that the model can handle a variety of subject profiles without overfitting to any particular population. We observed performance improvements in F1 scores, accuracy and specificity in all groups, particularly in mild cases and older age groups, confirming that the method works effectively even with varied patient characteristics.

Regarding the medication status, we evaluated the model separately on data from patients in their “On” and “Off” medication states. Patients in the “On” state generally show fewer motor symptoms due to the effects of dopaminergic treatment, while the “Off” state is marked by more pronounced motor symptoms, including fluctuations. Interestingly, when both “On” and “Off” states were combined during training, the model demonstrated superior results by better capturing the intra-patient variability between medicated and unmedicated states (Random group-2). This suggests that LIFT-PD can adapt to fluctuating motor symptoms effectively, providing accurate detection across different medication states, which

is critical for real-world clinical monitoring and intervention planning.

B. Compare with State-of-the-Art Models

Table VII compares the performance of our LIFT-PD model with state-of-the-art methods for detecting FoG in PD patients. Although the Multi-head CNN [12] achieves the highest detection rates for FoG episodes (97.27%) and windows (94.64%), its precision (0.545) and specificity (0.491) are low, indicating a high false positive rate. High false positives can reduce the effectiveness of cueing due to patients’ adaptiveness to “always on” interventions [28] [29]. The one-class classifier [10] shows high precision (0.856) and specificity (0.891) but lower recall (0.716), missing many true FoG events, which can lead to inadequate monitoring and delayed interventions. The semi-supervised model [11] shows a recall around 12% lower and specificity approximately 13% lower than LIFT-PD, making it less suitable for in-home monitoring with a single accelerometer.

TABLE VII: Comparison with state-of-the-art models

Study	DFE	Rec/Sens/DFW	Prec	F1 Score	Spec.
One Class Classifier [10]	90.8%	71.6%	0.86	0.77	0.89
Semi-Supervised Model [11]	–	72.3%	–	–	0.71
Multi-head CNN [12]	97.3%	94.6%	0.56	0.68	0.49
LIFT-PD	88%	84%	0.74	0.79	0.82

Our LIFT-PD model achieves a balanced performance with 88% episode detection, 83.85% window detection, 0.74 precision, 0.84 recall, 0.79 F1-score, and 0.82 specificity. These results show that LIFT-PD achieves comparable performance

to the supervised methods while being more suitable for real-time wearable deployment with limited computational resources for remote monitoring.

C. Duration Based FoG Episode

Table VIII presents the detection rates for FoG episodes and windows, along with associated latency metrics, grouped into short, medium, and long durations. Our SSL model’s performance is compared with a baseline supervised model (metrics in parentheses).

The SSL model shows robust performance across all durations, with detection rates increasing as the episode lengthens. This trend is mirrored in the baseline model’s performance, indicating a consistent improvement across different modeling approaches. For short episodes, the detection rate is 83.3% for episodes and 68% for windows, with an average latency of 2.42 ± 0.45 seconds. For long episodes, these rates rise to 100% for episodes and 91.1% for windows, with a latency of 2.64 ± 1.45 seconds. The increasing detection rates for longer episodes are due to the more prominent and persistent FoG characteristics, such as tremors and shuffling gait, which the SSL model effectively captures. The increasing detection rates for longer episodes are due to the more prominent and persistent FoG characteristics, such as tremors and shuffling gait, which LIFT-PD effectively captures.

TABLE VIII: Duration-based FoG episode analysis.

Duration	FoG Episodes & windows detection rate (%) with latency (s) and standard deviation		
	Small, 0–6 s	Medium, 6–12 s	Large, >12 s
FoG Episodes	83.3% (82.8%)	100% (98.8%)	100% (100%)
FoG Windows	68% (71.4%)	81.9% (84.1%)	91.1% (92.6%)
Avg. Latency \pm SD	2.42 ± 0.45 s (2.38 ± 0.45 s)	2.6 ± 0.96 s (2.5 ± 0.82 s)	2.64 ± 1.45 s (2.6 ± 1.29 s)
Max. Latency	4.5 s (4.5 s)	6 s (5.25 s)	9.75 s (9.75 s)

Latency, representing the detection delay from episode onset, slightly increases with duration. Small episodes have an average latency of 2.42 ± 0.45 seconds, while long episodes reach 2.64 ± 1.45 seconds. Maximum latency values increase from 4.5 seconds for small episodes to 9.75 seconds for long ones, reflecting the need to analyze more data over time to confidently detect FoG onset. Despite this latency increase, the detection accuracy for longer episodes remains superior, showing the SSL model’s effectiveness in real-world applications by balancing latency and accuracy for reliable FoG detection across varying episode durations.

D. Threshold Effect in MAM

To determine the optimal activity threshold for the MAM, we evaluated the impact of different threshold values on various performance metrics, as presented in Table IX and Fig. 7. As observed in Table IX, lowering the activity threshold (e.g., 0.0) results in higher sensitivity (0.884) and higher detected FoG episode (DFE) rate (0.92), indicating that more

FoG events are detected. However, this comes at the cost of lower specificity (0.78) and a higher inference time (3.31 ms) due to the SSL model being activated more frequently, even during inactive periods. Conversely, increasing the activity threshold (e.g., 1.2) leads to higher specificity (0.846) and a lower rejection ratio (0.59), implying that fewer false positive detections occur during inactive periods. However, this improvement is accompanied by a slight decrease in sensitivity (0.845), DFE rate (0.809), and an increase in the number of missed FoG events.

TABLE IX: Effect of different activation thresholds on MAM

Threshold	Sens	Spec	DFE	Rejection Ratio	Inference Time
0	0.884	0.78	0.92	0	3.31 ms
0.2	0.87	0.75	0.92	0.17	1.96 ms
0.4	0.839	0.764	0.896	0.25	1.76 ms
1.2	0.845	0.846	0.809	0.59	1.1 ms

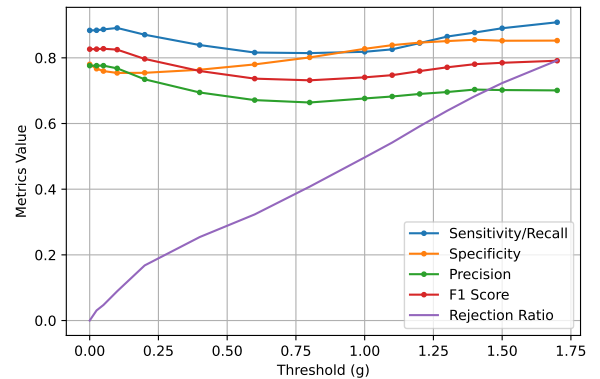


Fig. 7: Impact of activity threshold on SSL performance

Fig. 7 shows how metrics like specificity and rejection ratio increase steadily with the threshold, while sensitivity and overall detection performance (F1 score) gradually decline. Careful selection of the threshold is crucial to balance the requirements of accurately detecting active periods while effectively rejecting inactive intervals to optimize computational resources.

Fig. 9 shows that as the activity threshold increases, the model execution time decreases for both supervised and self-supervised models. At a threshold of 1.2g, the SSL model’s execution time reaches approximately 1.1 ms (Table IX, Fig. 9). This reduction is due to the MAM effectively filtering out inactive periods, reducing the need for the computationally intensive SSL model. The SSL model has slightly higher inference times than the supervised model due to an additional MLP layer on top of the pre-trained encoder. Despite the modest increase, the SSL model demonstrates enhanced robustness and superior performance using only 40-60% of labeled training data. The average execution time per window is 0.0295 ms for the supervised model and 0.0379 ms for the SSL model.

E. Effect of Labels During Pre-training

Fig. 8 illustrates how varying the label ratio (on the x-axis) impacts the performance (on the y-axis) of the self-supervised learning (SSL) and supervised models during training.

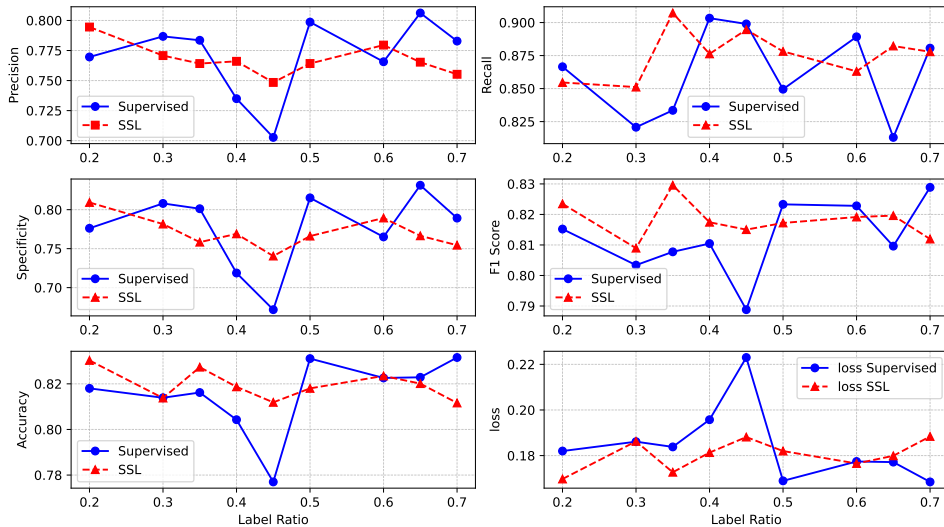


Fig. 8: Performance analysis for different amounts of labeled data.

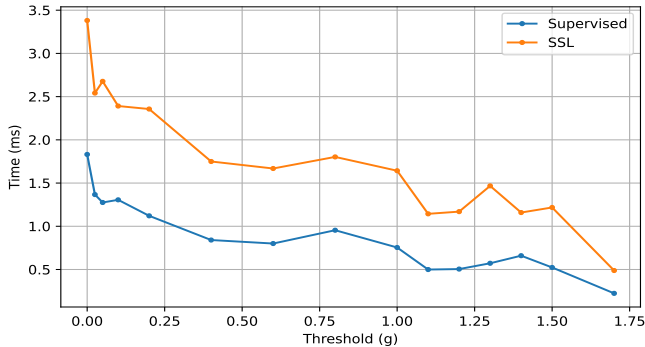


Fig. 9: Effect of activity threshold on inference time

As the ratio increases from 0.2 to 0.7, (meaning more labeled data is available for training), both models generally show an upward trend in metrics such as precision, recall, F1-score, and accuracy, which aligns with the expected behavior when more labeled data is available. However, a notable observation was the SSL model’s superior stability and consistency compared to the supervised counterpart, which displayed sharper performance fluctuations across different label ratios. This steadiness underscores the SSL model’s robustness and reduced sensitivity to the availability of labeled data during training. It also highlights the model’s capability to leverage pre-training on unlabeled data to learn generalized features transferable to the target task.

Fig. 8 also shows that SSL model not only competes closely but sometimes outperforms the supervised model, especially with 40-60% labeled data. This indicates that the SSL model can achieve promising results with fewer labeled instances, making it highly efficient and adaptable for scenarios where obtaining large amounts of labeled data is challenging.

F. Post Processing

The post-processing analysis evaluated the temporal dynamics between false positives (FPs) and true FoG episodes (TFE) detected by the LIFT-PD framework.

On average, FPs occurred 16 seconds after the previous TFE and 18.5 seconds before the next true episode, suggesting they

often arise from residual motor instability or sensor inaccuracies immediately following an actual FoG event. Our ‘Pre FP Analysis’ shows that FPs were found to occur approximately 14 seconds away from the nearest TFE, indicating the system’s high sensitivity to subtle motor pattern changes preceding or following a FoG episode. These false alarms could serve as precursors or warnings of impending FoG events, providing valuable time windows for treatment adjustments.

To address isolated false detections, a majority voting scheme was implemented. If a window’s classification differed from its immediate neighbors, it was adjusted to match them, smoothing the detection sequence. This approach improved the detection performance, increasing the detected true FoG episodes from 88% to 89.8% and true FoG windows from 83.85% to 84.64%.

V. DISCUSSION & CONCLUSION

In this study, we introduced LIFT-PD, a computationally simple self-supervised learning framework for real-time and patient-independent detection of Freezing of Gait (FoG) episodes in patients with Parkinson’s Disease (PD). LIFT-PD addresses critical challenges in continuous, in-home monitoring by eliminating the need for extensive labeled data, employing a unique *differential hopping windowing technique* to handle imbalanced datasets, and optimizing power consumption through *opportunistic model activation*. Our results show that LIFT-PD achieves performance comparable to the state-of-the-art methods while consuming less power and needing fewer annotated training samples, making it effective, generalizable, and suitable for deployment on wearable devices. Its ability to function with minimal data annotation and handle imbalanced datasets reduces the burden on healthcare providers, improving cost-effectiveness. It uses a single triaxial accelerometer, operates directly on raw sensor data without extensive preprocessing, and selectively activates the model only during active periods, significantly enhancing energy efficiency. By relying on a single, easily wearable sensor, the system enhances patient comfort, making it feasible for continuous, real-world monitoring in home environments.

From a clinical perspective, LIFT-PD can play a crucial role in the management of FoG, which is often unresponsive to traditional PD medications. Accurate detection of FoG events, as demonstrated by LIFT-PD, allows for the timely delivery of external cues, such as rhythmic tones or vibrotactile stimulation, which can help break or prevent FoG episodes without causing habituation. This targeted cueing approach enhances treatment efficacy and supports more personalized interventions [3], [30]. The system's real-time, continuous monitoring capability using a single triaxial accelerometer makes it practical for in-home use, providing clinicians with more comprehensive data on the patient's condition outside clinical settings.

Overall, LIFT-PD provides a practical, real-world solution for FoG detection, improving PD management, and improving patient quality of life. By providing continuous, real-time monitoring in home environments, the system supports more accurate assessments of a patient's condition outside of clinical settings.

REFERENCES

- [1] A. Nieuwboer and N. Giladi, "Characterizing freezing of gait in parkinson's disease: models of an episodic phenomenon," *Movement Disorders*, vol. 28, no. 11, pp. 1509–1519, 2013.
- [2] L.-L. Zhang, S. D. Canning, and X.-P. Wang, "Freezing of gait in parkinsonism and its potential drug treatment," *Current neuropharmacology*, vol. 14, no. 4, p. 302, 2016.
- [3] C. Cosentino, M. Putzolu, S. Mezzarobba, M. Cecchella, T. Innocenti, G. Bonassi, A. Botta, G. Lagravinese, L. Avanzino, and E. Pelosin, "One cue does not fit all: a systematic review with meta-analysis of the effectiveness of cueing on freezing of gait in parkinson's disease," *Neuroscience & Biobehavioral Reviews*, p. 105189, 2023.
- [4] P. L. Jadhvani and P. Harjpal, "A review of artificial intelligence-based gait evaluation and rehabilitation in parkinson's disease," *Cureus*, vol. 15, no. 10, 2023.
- [5] L. Borzi, I. Mazzetta, A. Zampogna, A. Suppa, G. Olmo, and F. Irrera, "Prediction of freezing of gait in parkinson's disease using wearables and machine learning," *Sensors*, vol. 21, no. 2, p. 614, 2021.
- [6] T. Bikias, D. Iakovakis, S. Hadjidimitriou, V. Charisis, and L. J. Hadjileontiadis, "Deepfog: an imu-based detection of freezing of gait episodes in parkinson's disease patients via deep learning," *Frontiers in Robotics and AI*, vol. 8, p. 537384, 2021.
- [7] A. L. S. de Lima, L. J. W. Evers, T. Hahn, L. Bataille, J. L. Hamilton, M. A. Little, Y. Okuma, B. R. Bloem, and M. J. Faber, "Freezing of gait and fall detection in parkinson's disease using wearable sensors: a systematic review," *Journal of Neurology*, vol. 264, pp. 1642 – 1654, 2017. [Online]. Available: <https://api.semanticscholar.org/CorpusID:3626185>
- [8] N. Peppes, P. Tsakanikas, E. Daskalakis, T. Alexakis, E. Adamopoulou, and K. Demestichas, "Foggan: Generating realistic parkinson's disease freezing of gait data using gans," *Sensors*, vol. 23, no. 19, p. 8158, 2023.
- [9] L. Sigcha, L. Borzi, I. Pavón, N. Costa, S. Costa, P. Arezes, J. M. López, and G. De Arcas, "Improvement of performance in freezing of gait detection in parkinson's disease using transformer networks and a single waist-worn triaxial accelerometer," *Engineering Applications of Artificial Intelligence*, vol. 116, p. 105482, 2022.
- [10] N. Naghavi and E. Wade, "Towards real-time prediction of freezing of gait in patients with parkinson's disease: a novel deep one-class classifier," *IEEE Journal of Biomedical and Health Informatics*, vol. 26, no. 4, pp. 1726–1736, 2021.
- [11] V. Mikos, C.-H. Heng, A. Tay, N. S. Y. Chia, K. M. L. Koh, D. M. L. Tan, and W. L. Au, "Real-time patient adaptivity for freezing of gait classification through semi-supervised neural networks," in *2017 16th IEEE International Conference on Machine Learning and Applications (ICMLA)*. IEEE, 2017, pp. 871–876.
- [12] L. Borzi, L. Sigcha, D. Rodríguez-Martín, and G. Olmo, "Real-time detection of freezing of gait in parkinson's disease using multi-head convolutional neural networks and a single inertial sensor," *Artif. Intell. Med.*, vol. 135, no. C, jan 2023. [Online]. Available: <https://doi.org/10.1016/j.artmed.2022.102459>
- [13] T. Chen, S. Kornblith, M. Norouzi, and G. Hinton, "A simple framework for contrastive learning of visual representations," 2020.
- [14] B. Khaertdinov, E. Ghaleb, and S. Asteriadis, "Contrastive self-supervised learning for sensor-based human activity recognition," in *2021 IEEE International Joint Conference on Biometrics (IJCB)*. IEEE, 2021, pp. 1–8.
- [15] A. Mamun, C.-C. Kuo, D. W. Britt, L. D. Devoe, M. I. Evans, H. Ghasemzadeh, and J. Klein-Seetharaman, "Neonatal risk modeling and prediction," in *2023 IEEE 19th International Conference on Body Sensor Networks (BSN)*. IEEE, 2023, pp. 1–4.
- [16] R. R. Azghan, N. C. Glodosky, R. K. Sah, C. Cuttler, R. McLaughlin, M. J. Cleveland, and H. Ghasemzadeh, "Personalized modeling and detection of moments of cannabis use in free-living environments," in *2023 IEEE 19th International Conference on Body Sensor Networks (BSN)*, 2023, pp. 1–4.
- [17] J. Wang, T. Zhu, J. Gan, L. L. Chen, H. Ning, and Y. Wan, "Sensor data augmentation by resampling in contrastive learning for human activity recognition," *IEEE Sensors Journal*, vol. 22, no. 23, pp. 22994–23008, 2022.
- [18] Z. Liu, A. Alavi, M. Li, and X. Zhang, "Self-supervised contrastive learning for medical time series: A systematic review," *Sensors*, vol. 23, no. 9, p. 4221, 2023.
- [19] W. Zhang, Z. Yang, H. Li, D. Huang, L. Wang, Y. Wei, L. Zhang, L. Ma, H. Feng, J. Pan *et al.*, "Multimodal data for the detection of freezing of gait in parkinson's disease," *Scientific data*, vol. 9, no. 1, pp. 1–10, 2022.
- [20] Y. Guo, D. Huang, W. Zhang, L. Wang, Y. Li, G. Olmo, Q. Wang, F. Meng, and P. Chan, "High-accuracy wearable detection of freezing of gait in parkinson's disease based on pseudo-multimodal features," *Computers in Biology and Medicine*, vol. 146, p. 105629, 2022.
- [21] A. Howard, A. Salomon, E. Gazit, HCL-Jevster, J. Hausdorff, L. Kirsch, Maggie, P. Ginis, R. Holbrook, and Y. F. Karim, "Parkinson's freezing of gait prediction," Kaggle, 2023. [Online]. Available: <https://kaggle.com/competitions/tlvmc-parkinsons-freezing-gait-prediction>
- [22] T. Reches, M. Dagan, T. Herman, E. Gazit, N. A. Gouskova, N. Giladi, B. Manor, and J. M. Hausdorff, "Using wearable sensors and machine learning to automatically detect freezing of gait during a fog-provoking test," *Sensors*, vol. 20, no. 16, p. 4474, 2020.
- [23] B. Manor, M. Dagan, T. Herman, N. A. Gouskova, V. G. Vanderhorst, N. Giladi, T. G. Trivison, A. Pascual-Leone, L. A. Lipsitz, and J. M. Hausdorff, "Multitarget transcranial electrical stimulation for freezing of gait: a randomized controlled trial," *Movement Disorders*, vol. 36, no. 11, pp. 2693–2698, 2021.
- [24] K. Ziegler, F. Schroeteler, A. O. Ceballos-Baumann, and U. M. Fietzek, "A new rating instrument to assess festination and freezing gait in parkinsonian patients," *Movement Disorders*, vol. 25, no. 8, pp. 1012–1018, 2010.
- [25] I. R. Rahman, S. B. Soumma, and F. B. Ashraf, "Machine learning approaches to metastasis bladder and secondary pulmonary cancer classification using gene expression data," in *2022 25th International Conference on Computer and Information Technology (ICCIT)*, 2022, pp. 430–435.
- [26] D. Roggen, M. Plotnik, and J. Hausdorff, "Daphnet Freezing of Gait," UCI Machine Learning Repository, 2010, DOI: <https://doi.org/10.24432/C56K78>.
- [27] M. Malekzadeh, R. G. Clegg, A. Cavallaro, and H. Haddadi, "Mobile sensor data anonymization," in *Proceedings of the International Conference on Internet of Things Design and Implementation*, ser. IoTDI '19. New York, NY, USA: ACM, 2019, pp. 49–58. [Online]. Available: <http://doi.acm.org/10.1145/3302505.3310068>
- [28] P. Ginis, E. Nackaerts, A. Nieuwboer, and E. Heremans, "Cueing for people with parkinson's disease with freezing of gait: a narrative review of the state-of-the-art and novel perspectives," *Annals of physical and rehabilitation medicine*, vol. 61, no. 6, pp. 407–413, 2018.
- [29] E. Cubo, S. Leurgans, and C. G. Goetz, "Short-term and practice effects of metronome pacing in parkinson's disease patients with gait freezing while in the 'on' state: randomized single blind evaluation," *Parkinsonism & related disorders*, vol. 10, no. 8, pp. 507–510, 2004.
- [30] A. Nieuwboer, "Cueing for freezing of gait in patients with parkinson's disease: a rehabilitation perspective," *Movement disorders: official journal of the Movement Disorder Society*, vol. 23, no. S2, pp. S475–S481, 2008.



Shovito Barua Soumma, BS, (Student Member, IEEE) received his BS degree in Computer Science from the Bangladesh University of Engineering & Technology (BUET), Dhaka, Bangladesh, in 2022. Currently, he is working toward the PhD degree in Biomedical Informatics at Arizona State University. He is interested in digital health, embedded system, machine learning and explainable AI. The focus of his research is on design and development of power efficient AI models for wearable monitoring systems with various applications in healthcare.

tems with various applications in healthcare.



Kartik Mangipudi, MD, is an Assistant Professor of Neurology at the University of Florida. He received his medical degree from the Royal College of Surgeons Ireland and completed his transitional year, neurology residency and movement disorders fellowship at Mayo Clinic, Arizona. His clinical and research interests are focused on better understanding and quantifying gait disorders.



Shyamal Mehta, MD, PhD, is an Associate Professor of Neurology at the Mayo Clinic, Arizona. During his career as a clinician-researcher, has focused his efforts on various aspects of Parkinson's disease. He is engaged in research using deep brain stimulation and has published on the effects of deep brain stimulation on cognition in Parkinson's disease. He has an ongoing collaboration at Arizona State University for research in gait dysfunction in Parkinson's disease and has published several papers in that area. Dr. Mehta

also serves as site principal investigator on several pharmaceutically funded clinical trials related to Parkinson's disease, and for chemodenervation using botulinum toxin injections. Currently, he is engaged in artificial intelligence research to improve Parkinson's disease diagnosis.



Daniel Peterson, PhD, is an associate professor of nutrition and health promotion at Arizona State University. His current research focuses on understanding the interaction between balance, postural control and cognitive deficits in people with neurological disorders such as Parkinson's and multiple sclerosis. His goal is to understand why people fall and how to prevent falls. He focuses on three areas: the mechanics of how people fall; the underlying neural control of movements related to falls; and the development

of interventions to prevent falls. Dr. Peterson earned a master's in kinesiology at Pennsylvania State University and a master's in clinical investigation and a doctorate in movement science at Washington University in St. Louis. He completed postdoctoral training in neurology at Oregon Health & Science University



Hassan Ghasemzadeh, PhD (Senior Member, IEEE), received the BSc degree from the Sharif University of Technology, Tehran, Iran, in 1998, the MSc degree from the University of Tehran, Tehran, Iran, in 2001, and the PhD degree from the University of Texas at Dallas, Richardson, TX, in 2010, all in computer engineering. He was on the faculty of Azad University from 2003-2006 where he served as founding chair of the Computer Science and Engineering Department at the Damavand branch, Tehran, Iran. He spent

the academic year 2010- 2011 as a postdoctoral fellow at the West Wireless Health Institute, La Jolla, CA. He was a research manager at the UCLA Wireless Health Institute in 2011-2013. Currently he is an associate professor of biomedical informatics, the director of undergraduate biomedical informatics program, and a graduate faculty of computer science, computer engineering, and biomedical engineering at Arizona State University (ASU). Prior to joining ASU, he was an assistant/associate professor of computer science at Washington State University (WSU 2014-2021). The focus of his research is on algorithm design and system level optimization of embedded and pervasive systems with applications in healthcare and wellness.